



Self-scaling generalized Townsend-Perry constants for high-order moments in turbulent boundary layers

Xibo He  and Hongyou Liu ^{*}

Center for Particle-Laden Turbulence, *Lanzhou University*, Lanzhou 730000, People's Republic of China

Xiaojing Zheng 

Research Center for Applied Mechanics, *Xidian University*, Xi'an 710071, People's Republic of China



(Received 29 April 2024; accepted 5 August 2024; published 22 August 2024)

Inspired by the thought-provoking paper of Meneveau and Marusic [*J. Fluid Mech.* **719**, R1 (2013)], the universal expression of the self-scaling generalized Townsend-Perry constants for the high-order statistical moments is investigated. The measured results deviate from the previous attached-eddy-model-based Gaussian prediction because the wall-non-attached eddies with sub-Gaussian statistics mask the Gaussian behavior of the wall-attached eddies. Leveraging the generalized Gaussian distribution function and the logarithmic law for turbulence intensity, the universal expression of the self-scaling generalized Townsend-Perry constants, regardless of the eddy type, is derived. Moreover, asymptotic expression of the shape parameter in self-scaling generalized Townsend-Perry constants with Reynolds number is further characterized by data in boundary layers and atmospheric surface layers with Reynolds number Re_τ spanning over $O(10^3)$ to $O(10^6)$.

DOI: [10.1103/PhysRevFluids.9.L082602](https://doi.org/10.1103/PhysRevFluids.9.L082602)

Introduction. High-Reynolds-number turbulent boundary layers are ubiquitous in nature and industrial applications. A universal feature of these flows, and one that is extensively relied upon for modeling purposes, is the logarithmic law. In the logarithmic layer, the logarithmic law as a function of the distance from the wall z applies for the streamwise mean velocity U [1,2],

$$U^+ = \frac{1}{\kappa} \ln(z^+) + B, \quad (1)$$

where $U^+ \equiv U/U_\tau$ and $z^+ \equiv zU_\tau/\nu$. U_τ , ν and κ are the friction velocity, kinetic viscosity and Kármán constant, respectively. B is a parameter dependent on the roughness of the wall.

Another notable nature is the log behavior for the streamwise velocity variance in boundary layers. Townsend [3] proposed that the flow field is occupied by an array of wall-attached, self-similar, energy-containing eddies. Their sizes are proportional to z , and the population density inversely varies with the size and hence with z . A phenomenological model of wall-attached eddies was then proposed based on Townsend's attached eddy hypothesis (AEH) and called the attached eddy model (AEM). Following the AEM to its logical conclusion, when the scale separation is sufficient (i.e., in high-Reynolds-number flows), the streamwise velocity variance (turbulence intensity) is a logarithmic function of the wall-normal distance z , i.e.,

$$\langle u^2 \rangle^+ = B_1 - A_1 \ln(z/\delta), \quad (2)$$

where δ is the outer length scale, which is the boundary-layer thickness, channel half-height, and pipe radius for the turbulent boundary layer (TBL), channel, and pipe flows, respectively. A_1 is called

^{*}Contact author: liuhongyou@lzu.edu.cn

the Townsend-Perry constant, and B_1 is a parameter dependent on the flow conditions and geometry. Valid supports for the existence of this logarithmic law have come from subsequent experimental studies [1,4–7].

Later, Meneveau and Marusic [8] extended the logarithmic law to the p th root of the $2p$ -order moments of streamwise velocity fluctuations and proposed the existence of generalized Townsend-Perry constants. The generalized logarithmic law for the high-order moments of the streamwise velocity fluctuations follows

$$\langle u^{+2p} \rangle^{1/p} = B_p - A_p \ln(z/\delta), \quad (3)$$

where $2p$ ($p \geq 1$) is the moment order. For Gaussian statistics, the generalized Townsend-Perry constants A_p are expected to be $A_p = A_1[(2p-1)!!]^{1/p}$ ($!!$ is the double factorial), and B_p is the additive constant for high-order moments. However, although Meneveau and Marusic [8] validated the generalized logarithmic decay for high-order moments in TBLs at $2800 \leq Re_\tau \leq 19030$ ($Re_\tau \equiv \delta U_\tau/\nu$), the slopes A_p were found to be lower than the Gaussian prediction $A_1[(2p-1)!!]^{1/p}$. This deviation (sub-Gaussian behavior) indicates the insufficiency of the Gaussian distribution. Subsequently, the logarithmic decay for high-order moments and the deviation behavior of measured generalized Townsend-Perry constants A_p from the Gaussian prediction were widely found in experiments [9–11]. Notably, a multitude of coexisting eddies of different types are filled in high-Reynolds-number flows, the eddies that cannot be described by the AEM (e.g., the global model motions described in Baars and Marusic [12]) and the interaction [13] may have an impact on the predicted generalized Townsend-Perry constants A_p . In this scenario, taking these factors into consideration, high-Reynolds-number data with larger scale separation and a suitable separation method are desired to investigate this issue.

In the following, high Re_τ [$\sim O(10^6)$] synchronous observational atmospheric surface layer (ASL) data are used here to determine the existence of (sub-) Gaussian statistics in (3), and the universal expression of the self-scaling generalized Townsend-Perry constants A_p/A_1 are determined based on the theoretical analysis and experimental validation.

Experimental data. The dataset employed in this study is acquired from Liu *et al.* [14] at Reynolds number $Re_\tau \sim O(10^6)$ measured at the Qingtu Lake Observation Array (QLOA) site in western China, using a wall-normal array of eleven sonic anemometers under near-neutral stratification conditions. Detailed information on the experimental setup and data preprocessing can be found in Wang and Zheng [6]. Additional data used for determining the parameter are from the High Reynolds Number Boundary Layer Wind Tunnel (HRNBLWT) [8] at the University of Melbourne, with Reynolds numbers $Re_\tau = 2800, 3900, 7300$, and 19030 .

First, the basic statistical properties of the data from the QLOA observation are supplied. As a representative case, the result at $z/\delta = 0.0114$ is taken as an example to show the probability density function (PDF) of the streamwise velocity fluctuation u . The observational results are shown in Fig. 1(a) by the black filled symbols; moreover, the standard Gaussian distribution [red curve in Fig. 1(a)] is supplied for comparison. The hyper- and sub-Gaussian distributions are also added in Fig. 1(a); the corresponding definition can be found later. It can be seen that the observational result is close to Gaussian distribution, but a deviation around the maximum value from the Gaussian behavior can be found, which is fairly consistent with the TBL results from Vallikivi *et al.* [9]. In addition, the tail of the measured PDF $P(u^+)$ is slightly lower than that of the standard Gaussian distribution towards the tail of the sub-Gaussian distribution. Next, to further evaluate the statistical convergence of the data, the premultiplied PDFs of the streamwise velocity fluctuations are examined based on the PDF $P(u^+)$. Premultiplied PDFs for $2p = 2, 4, 6, 8$, and 10 are shown in Fig. 1(b). In the premultiplied form, the area under the curve represents the magnitude of the corresponding moment. Theoretically, for the Gaussian distribution, its higher-order premultiplied PDF is symmetric. However, since the measured results do not strictly satisfy the Gaussian distribution [as shown in Fig. 1(a)], the corresponding premultiplied higher-order PDF inevitably exhibits asymmetry to some extent. It can be seen that the curves for $2p = 2, 4$,

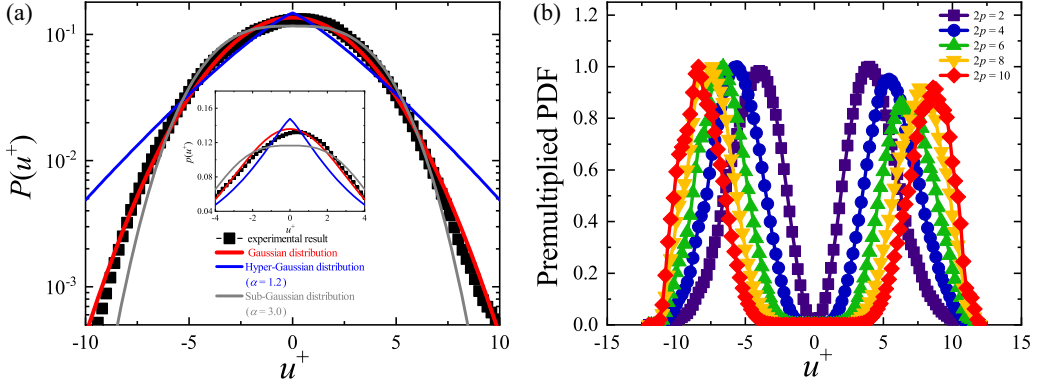


FIG. 1. (a) Probability density function (PDF) for the ASL at a height of $z/\delta = 0.0114$; \blacksquare , $P(u^+)$; the red, blue, and gray curves represent Gaussian, hyper-Gaussian, and sub-Gaussian distribution, respectively. (b) Premultiplied PDF of normalized velocity fluctuations $u^{+2p}P(u^+)$ for the ASL dataset, at a height of $z/\delta = 0.0114$. Different moments are represented as $2p = 2$ (\blacksquare), $2p = 4$ (\bullet), $2p = 6$ (\blacktriangle), $2p = 8$ (\blacktriangledown), and $2p = 10$ (\blacklozenge). Each curve has been normalized by its peak for plotting purposes.

6, 8, and 10 show acceptable “closure” from the premultiplied PDFs [8]. This indicates that every higher-order moment of the streamwise velocity fluctuations is well-captured by the amount of the data available, which enables further investigation of the self-scaling generalized Townsend-Perry constants for high-order moments of the streamwise velocity fluctuations.

Results: High-order moments for wall-attached and nonattached eddies. With the development of studies on coherent motions in wall turbulence, many researchers have suggested that the flow field not only includes eddies that can be described by the AEM, but also contains other large-scale energetic motions of other nature [12,15]. These coexisting eddies in high-Reynolds-number flows may cause the overall statistical characteristics of the flow field to deviate from the predicted tendency. As the Reynolds number increases, more abundant eddies with nonattached properties that deviate from the AEM prediction emerge in high-Reynolds-number wall-bounded flows. In this scenario, scholars have proposed many methodologies to separate/extract eddies satisfying the AEM [11,12,15]. In this study, the wall-coherent (wall-attached) signal $u_A(z; t)$ at different heights can be obtained by the spectral linear stochastic estimation (SLSE) technique [16]. The near-wall signal $u^+(z_R)$ [Fig. 2(a)] and the signal $u^+(z)$ [Fig. 2(b)] at a higher position are transformed into Fourier space to obtain the scale-dependent complex-valued kernel, $H(z_R, z; f)$, which is defined by

$$H(z_R, z; f) = \frac{\langle \hat{u}(z; f) \overline{\hat{u}(z_R; f)} \rangle}{\langle \hat{u}(z_R; f) \overline{\hat{u}(z_R; f)} \rangle} = |H(z_R, z; f)| e^{j\phi(z_R, z; f)}, \quad (4)$$

where $\langle \cdot \rangle$ denotes the ensemble average, the OverHat represents the Fourier transform, $|\cdot|$ designates the modulus, the overline indicates the complex conjugate, and $\phi(z_R, z; f)$ is the phase difference of the two spectra. The spectral domain estimate of the wall-coherent velocity of hierarchies of eddies above the near-wall reference height z_R can be expressed as

$$\hat{u}_A(z; f) = H(z_R, z; f) \hat{u}(z_R; f). \quad (5)$$

Finally, the time-domain conditional estimate is obtained by the inverse Fourier transform, $u_A(z; t) = \mathcal{F}^{-1}[\hat{u}_A(z; f)]$ [red line in Fig. 2(c)]. The entire decomposition procedure is presented by the diagram in Fig. 2(d). The analysis of the SLSE in this study follows the methods of Baars *et al.* [16] and Hu *et al.* [15], and there is no additional specific selection of data from which to choose the desired results in this study.

Based on this data-driven decomposition methodology (5), the coherent velocity u_A with wall-attachedness over the whole observational range can be obtained. These decomposed portions are

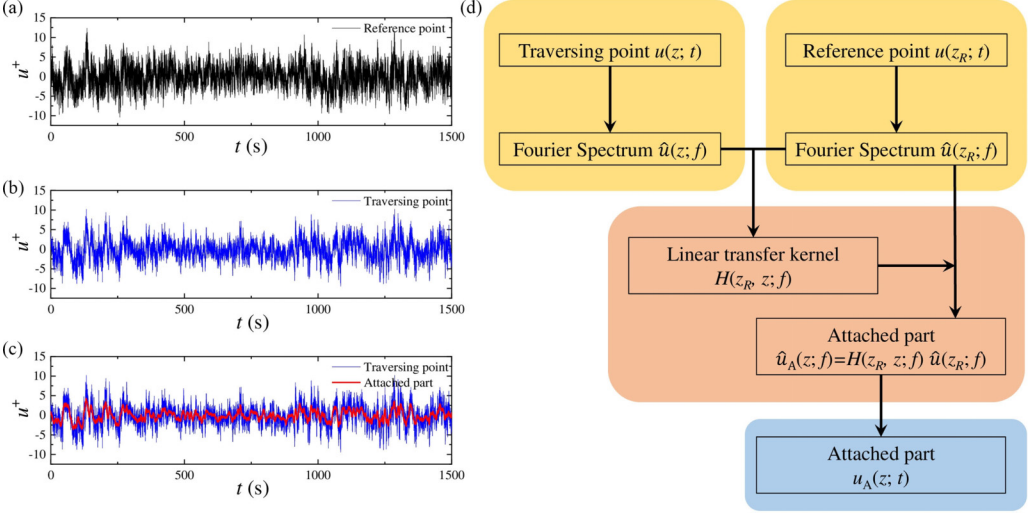


FIG. 2. (a) The fluctuating velocity signal at reference point z_R . (b) The fluctuating velocity signal at traversing point z . (c) The full-scale signal and the corresponding wall-attached signal at traversing point z . (d) Diagram of the decomposition procedure.

individually explored to evaluate their high-order moment characteristics ($2p = 2, 4, 6, 8$, and 10), and the results are shown in Fig. 3(a). Note that the moments for each order of the decomposed velocity fluctuations intuitively show log-linear decay in the logarithmic layer, which is quite similar to the “generalized logarithmic law” proposed by Meneveau and Marusic [8], i.e., satisfying Eq. (3). However, the decay slopes are quite different. Here, taking the moment order $2p = 2$

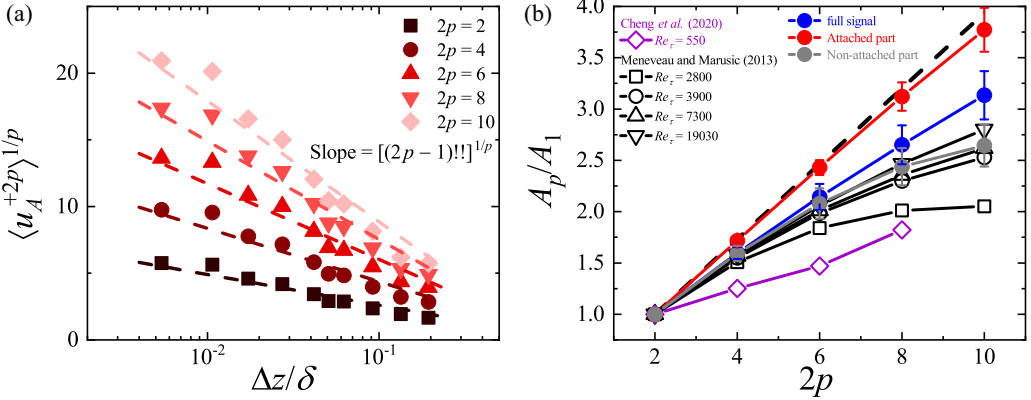


FIG. 3. (a) Moments of order $2p = 2$ (■), $2p = 4$ (●), $2p = 6$ (▲), $2p = 8$ (▼), and $2p = 10$ (◆) of decomposed streamwise velocity fluctuation u_A^+ as a function of wall-normal distance z/δ for the ASL dataset. The red dashed lines are the fitting lines with $A_p = [(2p-1)!!]^{1/p}$. (b) The self-scaling A_p/A_1 as a function of the moment order $2p$. The red filled symbols are results from the decomposed wall-attached portions, and the gray filled symbols are the results from the residual part. The black open, purple open, and blue filled symbols are the undecomposed results from Meneveau and Marusic [8], Cheng et al. [19], and QLOA, respectively. The error bars in the vertical axis represent the corresponding standard deviation for the datasets in similar conditions. The black dashed curve indicates the Gaussian values $A_p/A_1 = [(2p-1)!!]^{1/p}$.

as an example, the near universal slope $A_1 = 1.07$ for wall-attached portions is consistent with the turbulence intensity slope with z previously reported in Baars and Marusic [17] ($A_1 = 0.98$) and Hu *et al.* [15] ($A_1 = 1.0$). It shows that the decay slopes of the turbulence intensity for decomposed motions are generally invariant and are essentially free of Reynolds number effects [17], satisfying the description in the AEM [3]. This evidence suggests this data-driven method is effective in extracting wall-attached motions in this study. However, the decay slopes for the undecomposed fields are approximately 1.21–1.33 and have a weak Reynolds number dependence [4,6,18]. In addition, the decay slopes of the high-order moments for the decomposed portions [red symbols in Fig. 3(a)] can almost be described by the Gaussian prediction in Eq. (3) [red dashed line in Fig. 3(a)] with satisfying $A_p = A_1[(2p - 1)!!]^{1/p}$ in high-Reynolds-number flows. Since the magnitude of the decay slope A_1 (Townsend-Perry constant) is shown to be approximately 1 through both the decomposition method used in this study [Fig. 3(a)] and different decomposition methods previously reported [15,17], the generalized Townsend-Perry constants A_p can be expressed as $A_p = [(2p - 1)!!]^{1/p}$. In that way, the generalized logarithmic law Eq. (3) proposed by Meneveau and Marusic [8] in terms of describing the high-order statistical moments of wall-attached motions can be further written in a straightforward way as

$$\begin{aligned} \langle u_A^{+2p} \rangle^{1/p} &= C_p - A_p \ln(z/\delta) \\ &= C_p - [(2p - 1)!!]^{1/p} \ln(z/\delta), \end{aligned} \quad (6)$$

where C_p can be analogized to B_p in Eq. (3), which only depends on the flow conditions and geometry [8].

In addition, variations in the self-scaling decay slope A_p/A_1 for each high-order moment with order are further evaluated and are presented in Fig. 3(b). As predicted by Meneveau and Marusic [8], the tendency of Eq. (6) (black dashed line) is in good agreement with the variation of high-order moments for wall-attached motions (red line), which illustrates that Eq. (6) provides a good description of the high-order moment behavior of wall-attached motions. However, the result for the remaining nonattached portions [gray line in Fig. 3(b)] obtained through the decomposition still exhibits sub-Gaussian behavior, meaning that the nonattached-eddy contribution superposed on contribution $\langle u_A^{+2p} \rangle^{1/p}$ from wall-attached eddies masks the Gaussian behavior of the wall-attached eddies, thus giving rise to the measured sub-Gaussian statistics. In this scenario, the universal expression of the self-scaling generalized Townsend-Perry constants is desired to provide a good indication on the variation of the measured high-order statistics.

Universal expression of the self-scaling generalized Townsend-Perry constants: Theoretical analysis. Because the Gaussian distribution is not capable of characterizing the measured results, it is necessary to start with the most fundamental generalized Gaussian distribution function. The PDF for a generalized Gaussian distributed zero-mean random variable u with standard deviation σ is given by

$$P(u, \alpha, \beta) = \frac{\alpha}{2\beta\Gamma(1/\alpha)} e^{-(\frac{u}{\beta})^\alpha}, \quad (7)$$

where $\alpha > 0$ is the shape parameter, $\beta = \sigma \sqrt{\Gamma(1/\alpha)/\Gamma(3/\alpha)}$ is the scale parameter, and Γ is the gamma function [$\Gamma(x) = \int_0^{+\infty} t^{x-1} e^{-t} dt$, $x > 0$] [20,21]. Then, the k th moment of the random variable u can be expressed as

$$\begin{aligned} \langle u^k \rangle &= \int_{-\infty}^{+\infty} \frac{\alpha u^k}{2\beta\Gamma(1/\alpha)} e^{-(\frac{u}{\beta})^\alpha} du \\ &= \frac{\alpha\beta^k}{2\Gamma(1/\alpha)} \int_{-\infty}^{+\infty} \left(\frac{u}{\beta}\right)^k e^{-(\frac{u}{\beta})^\alpha} d\left(\frac{u}{\beta}\right). \end{aligned} \quad (8)$$

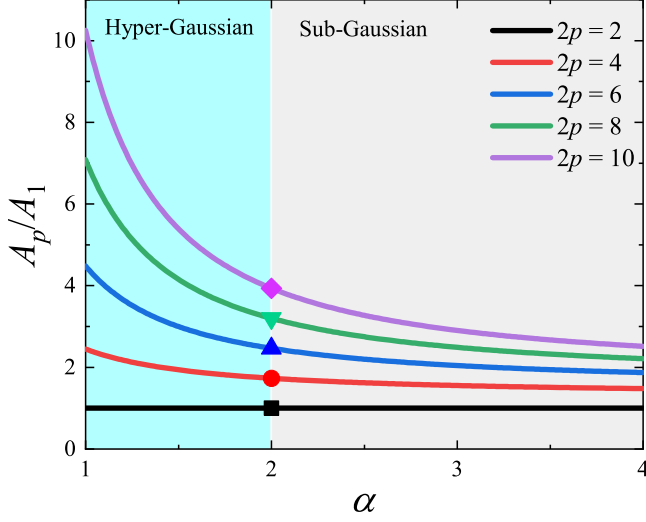


FIG. 4. The self-scaling generalized Townsend-Perry constants against α for $2p = 2$ to 10. The filled symbols of order $2p = 2$ (■), $2p = 4$ (●), $2p = 6$ (▲), $2p = 8$ (▼), and $2p = 10$ (◆) are $[(2p - 1)!!]^{1/p}$ as recorded in Meneveau and Marusic [8].

When k is odd,

$$\langle u^k \rangle = 0. \quad (9)$$

When k is even,

$$\langle u^k \rangle = \frac{\alpha \beta^k}{\Gamma(1/\alpha)} \int_0^{+\infty} \left(\frac{u}{\beta}\right)^k e^{-\left(\frac{u}{\beta}\right)^\alpha} d\left(\frac{u}{\beta}\right). \quad (10)$$

Let $(u/\beta)^\alpha = z$, and Eq. (10) can be written as

$$\begin{aligned} \langle u^k \rangle &= \frac{\beta^k}{\Gamma(1/\alpha)} \int_0^{+\infty} z^{\frac{k}{\alpha}} e^{-z} z^{\left(\frac{1}{\alpha}-1\right)} dz \\ &= \frac{\beta^k}{\Gamma(1/\alpha)} \Gamma\left(\frac{k+1}{\alpha}\right). \end{aligned} \quad (11)$$

Since k is even, let $k = 2p$. After simplification, Eq. (11) becomes

$$\langle u^{+2p} \rangle^{1/p} = \frac{\Gamma\left(\frac{2p+1}{\alpha}\right)^{1/p} \Gamma(1/\alpha)^{\frac{p-1}{p}}}{\Gamma(3/\alpha)} \sigma^{+2}. \quad (12)$$

Thus far, the relationship between the high-order moments and the 2nd moment (variance) of random variable u can be obtained. Combined with the logarithmic law in Eq. (2), the self-scaling generalized Townsend-Perry constants A_p/A_1 can be expressed as

$$A_p/A_1 = \frac{\Gamma\left(\frac{2p+1}{\alpha}\right)^{1/p} \Gamma(1/\alpha)^{\frac{p-1}{p}}}{\Gamma(3/\alpha)}. \quad (13)$$

The self-scaling generalized Townsend-Perry constants for $2p = 2, 4, 6, 8,$ and 10 are shown in Fig. 4. When $\alpha < 2$ (or $\alpha > 2$), the corresponding distribution is hyper-Gaussian (or sub-Gaussian). Their respective distributions can be found in Fig. 1(a).

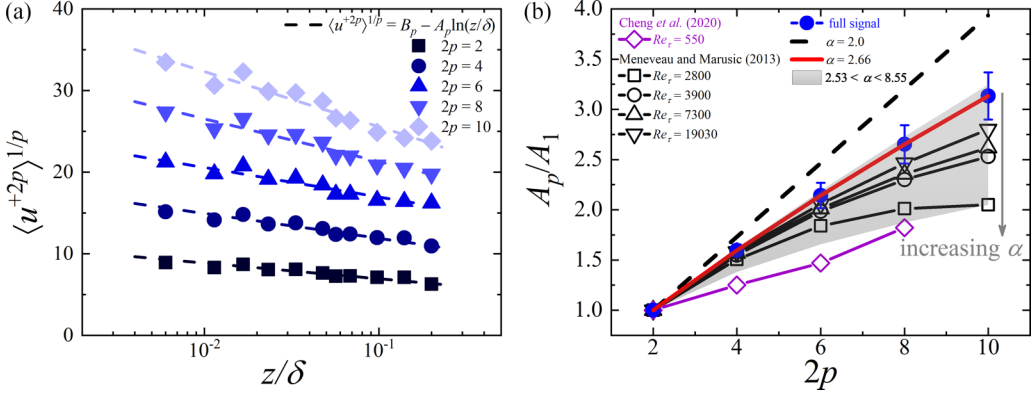


FIG. 5. (a) Moments of order $2p = 2$ (■), $2p = 4$ (●), $2p = 6$ (▲), $2p = 8$ (▼), and $2p = 10$ (◆) of streamwise velocity fluctuation as a function of wall-normal distance z/δ for the ASL dataset. Dashed lines are the fitting lines with Eq. (3). (b) The self-scaling A_p/A_1 as a function of the moment order $2p$; the symbols are as labeled in Fig. 3(b).

In particular, when $\alpha = 2$, the PDF of the random variable u follows a Gaussian distribution. Eq. (11) can be further simplified as

$$\begin{aligned} \langle u^k \rangle &= \frac{\beta^k}{\Gamma(1/2)} \Gamma\left(\frac{k+1}{2}\right) \\ &= (k-1)!! \sigma^k. \end{aligned} \quad (14)$$

Let $k = 2p$, and

$$\begin{aligned} \langle u^{+2p} \rangle^{1/p} &= [(2p-1)!!]^{1/p} \langle u^{+2} \rangle \\ &= [(2p-1)!!]^{1/p} [B_1 - A_1 \ln(z/\delta)] \\ &= B_p - A_p \ln(z/\delta). \end{aligned} \quad (15)$$

Equation (15) is the generalized logarithmic law expression of streamwise velocity fluctuations proposed by Meneveau and Marusic [8], where $A_p = A_1 [(2p-1)!!]^{1/p}$, as shown in Fig. 4 by filled symbols.

Empirical parameter and model validation. High even-order moments for $2p = 2, 4, 6, 8$, and 10 in near-neutral ASL are evaluated as a function of the wall-normal distance and are shown in Fig. 5(a). Every high-even-order moment in the logarithmic layer exhibits the “generalized logarithmic law” behavior proposed by Meneveau and Marusic [8], i.e., Eq. (3). Meneveau and Marusic [8] also predicted that the logarithmic decay slope A_p (generalized Townsend-Perry constants) of the streamwise velocity fluctuations with Gaussian distribution should satisfy $A_p = A_1 [(2p-1)!!]^{1/p}$, and the predicted tendency is shown in Fig. 5(b) as the black dashed line. As Meneveau and Marusic [8] noted, whether in TBL experiments [8,11,19] or in ASL observations, A_p/A_1 fails to collapse onto the predicted trend that assumes Gaussian statistics but is consistent with sub-Gaussian behavior. [In Eq. (13) for $2.53 < \alpha < 8.55$, as shown in the gray area in Fig. 5(b), in particular, the ASL result in this study can fairly satisfy the universal expression of the generalized logarithmic law expressed in Eq. (13) for $\alpha = 2.66$, as shown by the red line.]

In Eq. (12), the relationship between the high-order moments of the streamwise fluctuations u and second moment (variance) are obtained, which can effectively capture the statistical characteristics of the flow. However, it is important to note that there still exists a shape parameter α in Eq. (12) which needs a posteriori assessment. The exact expression form must be determined to refine the

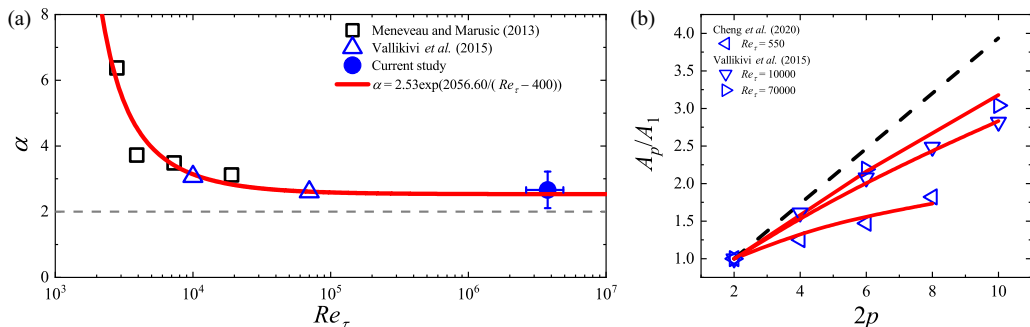


FIG. 6. (a) The shape parameter α versus Re_τ . The black open symbols (\square) are the results from Meneveau and Marusic [4], and the blue open symbols (Δ) are the results from Vallikivi *et al.* [9]. The blue filled symbol is the result from this study and the red curve is the asymptotic expression [Eq. (16)]. The error bars in the abscissa and ordinate axes represent the corresponding standard deviations of the Reynolds number and α for the datasets in similar conditions, respectively. (b) The self-scaling A_p/A_1 as a function of the moment order $2p$; the blue open symbols are the results from Cheng *et al.* [19] and Vallikivi *et al.* [9]. The red curves are the self-scaling generalized Townsend-Perry constants for the respective Reynolds number conditions calculated via Eqs. (13) and (16).

completeness of Eq. (12). Combining the high-quality experimental results [8] and observational result in this study, parametric equations are fitted and are given as [shown in Fig. 6(a)]

$$\alpha = 2.53 \exp \frac{2056.60}{Re_\tau - 400}, \quad (16)$$

where 400 is the asymptotic Reynolds number where the logarithmic layer dawns (i.e., $3Re_\tau^{1/2} = 0.15Re_\tau$) [4]. It can be easily seen that the coefficient 2.53 represents the asymptotic value for $Re_\tau \rightarrow \infty$. To present the validity of the asymptotic expression, several sets of data with different Reynolds numbers are employed. It can be seen that the results in Vallikivi *et al.* [9] agree well with the asymptotic expression in Eq. (16) in medium Reynolds number range [blue open symbol in Fig. 6(a)]. In addition, the self-scaling generalized Townsend-Perry constants reported earlier (in low Re condition [19] and in medium Re condition: [9]) show good agreement with the universal expression in Eq. (13) proposed in this study [red lines in Fig. 6(b)]. That is to say, the asymptotic expression in Eq. (16) is capable of describing the variation of parameter α , and the universal expression in Eq. (13) can effectively predict the measured self-scaling generalized Townsend-Perry constants spanning four to five orders of magnitude in the Reynolds number. It should be noted that the asymptotic value of α is 2.53, while the Gaussian distribution for α is 2. This difference indicates that the nonattached eddy contribution is nonnegligible for an asymptotic high Reynolds number, and AEM cannot provide a complete description of the full-scale flow field, especially in high-Reynolds-number conditions.

Concluding remarks. In conclusion, the self-scaling generalized Townsend-Perry constants A_p/A_1 for high-order moments in high-Reynolds-number turbulent boundary layers have been investigated. Nonattached eddies with sub-Gaussian statistics are found to mask the Gaussian behaviour of the wall-attached eddies in the flow field. In this scenario, the contribution for nonattached eddies is nonnegligible, and the attached eddy model is unable to describe the entire flow field, even in high-Reynolds-number flows. Leveraging the generalized Gaussian distribution function, the universal expression of the self-scaling generalized Townsend-Perry constants, regardless of the eddy type, is derived, i.e., $A_p/A_1 = \Gamma((2p+1)/\alpha)^{1/p} \Gamma(1/\alpha)^{\frac{p-1}{p}} \Gamma(3/\alpha)^{-1}$. Moreover, the asymptotic expression of the shape parameter α in self-scaling generalized Townsend-Perry constants is characterized by data in boundary layers and atmospheric surface layers with the Reynolds

number Re_τ spanning over $O(10^3)$ to $O(10^6)$. The expression can describe the measured sub-Gaussian behavior of high-order moments in a flow field.

The findings in this study may contribute additional insight into the fundamental statistical characteristics of coherent motions in flow fields and provide a good indication to test the accuracy of numerical simulations in high-Reynolds-number flows. It should also be noted that the present study further confirms that the attached eddy model cannot provide a complete description of the full-scale flow field. A universal physical expression (model) for the flow field is needed for future studies.

Acknowledgments. This study was supported by grants from the National Natural Science Foundation of China (Grants No. 12388101, No. 92052202, and No. 12372217). The authors would like to express their sincere appreciation for the support.

-
- [1] A. J. Smits, B. J. McKeon, and I. Marusic, High-Reynolds number wall turbulence, *Annu. Rev. Fluid Mech.* **43**, 353 (2011).
 - [2] J. Jiménez, Cascades in wall-bounded turbulence, *Annu. Rev. Fluid Mech.* **44**, 27 (2012).
 - [3] A. A. Townsend, *The Structure of Turbulent Shear Flow*, 2nd ed. edition (Cambridge University Press, 1976).
 - [4] I. Marusic, J. P. Monty, M. Hultmark, and A. J. Smits, On the logarithmic region in wall turbulence, *J. Fluid Mech.* **716**, R3 (2013).
 - [5] N. Hutchins, K. Chauhan, I. Marusic, J. Monty, and J. Klewicki, Towards reconciling the large-scale structure of turbulent boundary layers in the atmosphere and laboratory, *Boundary-Layer Meteorol.* **145**, 273 (2012).
 - [6] G. Wang and X. Zheng, Very large scale motions in the atmospheric surface layer: A field investigation, *J. Fluid Mech.* **802**, 464 (2016).
 - [7] R. Örlü, T. Fiorini, A. Segalini, G. Bellani, A. Talamelli, and P. H. Alfredsson, Reynolds stress scaling in pipe flow turbulence—first results from CICLoPE, *Phil. Trans. R. Soc. A* **375**, 20160187 (2017).
 - [8] C. Meneveau and I. Marusic, Generalized logarithmic law for high-order moments in turbulent boundary layers, *J. Fluid Mech.* **719**, R1 (2013).
 - [9] M. Vallikivi, M. Hultmark, and A. J. Smits, Turbulent boundary layer statistics at very high Reynolds number, *J. Fluid Mech.* **779**, 371 (2015).
 - [10] B. Birmir and X. Chen, Sub-Gaussian behavior of the Townsend-Perry constants in turbulent boundary layers, *Phys. Rev. E* **93**, 011101(R) (2016).
 - [11] L. Wang, C. Pan, J. Wang, and Q. Gao, Statistical signatures of u component wall-attached eddies in proper orthogonal decomposition modes of a turbulent boundary layer, *J. Fluid Mech.* **944**, A26 (2022).
 - [12] W. J. Baars and I. Marusic, Data-driven decomposition of the streamwise turbulence kinetic energy in boundary layers. Part 1. Energy spectra, *J. Fluid Mech.* **882**, A25 (2020).
 - [13] R. Mathis, N. Hutchins, and I. Marusic, Large-scale amplitude modulation of the small-scale structures in turbulent boundary layers, *J. Fluid Mech.* **628**, 311 (2009).
 - [14] H. Liu, G. Wang, and X. Zheng, Amplitude modulation between multi-scale turbulent motions in high-Reynolds-number atmospheric surface layers, *J. Fluid Mech.* **861**, 585 (2019).
 - [15] R. Hu, X. I. A. Yang, and X. Zheng, Wall-attached and wall-detached eddies in wall-bounded turbulent flows, *J. Fluid Mech.* **885**, A30 (2020).
 - [16] W. J. Baars, N. Hutchins, and I. Marusic, Spectral stochastic estimation of high-Reynolds-number wall-bounded turbulence for a refined inner-outer interaction model, *Phys. Rev. Fluids* **1**, 054406 (2016).
 - [17] W. J. Baars and I. Marusic, Data-driven decomposition of the streamwise turbulence kinetic energy in boundary layers. Part 2. Integrated energy and A_1 , *J. Fluid Mech.* **882**, A26 (2020).
 - [18] Y. Hwang, N. Hutchins, and I. Marusic, The logarithmic variance of streamwise velocity and conundrum in wall turbulence, *J. Fluid Mech.* **933**, A8 (2022).

- [19] C. Cheng, W. Li, A. Lozano-Durán, and H. Liu, Uncovering Townsend's wall-attached eddies in low-Reynolds-number wall turbulence, *J. Fluid Mech.* **889**, A29 (2020).
- [20] M. K. Varanasi and B. Aazhang, Parametric generalized Gaussian density estimation, *J. Acoust. Soc. Am.* **86**, 1404 (1989).
- [21] T. Wang, H. Li, Z. Li, and Z. Wang, A fast parameter estimation of generalized Gaussian distribution, in *Proceeding of the 2006 8th international Conference on Signal Processing* (IEEE, Beijing, 2006), pp. 101–104.